Iron-nickel bimetallic nanoparticles for reductive degradation of azo dye Orange G in aqueous solution

Alok D. Bokare [a], Rajeev C. Chikate [b], Chandrashekhar V. Rode [c], Kishore M. Paknikar [a,*]

[a] *Centre for Nanobioscience, Agharkar Research Institute, G. G. Agarkar Road, Pune 411004, India*
[b] *Department of Chemistry, MES Abasaheb Garware College, Karve Road, Pune 411004, India*
[c] *Chemical Engineering and Process Development Division, National Chemical Laboratory, Pune 411008, India*

Abstract

The degradation of Orange G, a monoazo dye, in aqueous solutions was investigated using Fe-Ni bimetallic nanoparticles. Transmission electron microscopy (TEM) of as-synthesized nanoparticles showed the presence of spherical particles having a size of 20–40 nm. X-ray photoelectron spectroscopy (XPS) did not detect the presence of nickel on the nanoparticle surface, which suggested a uniform distribution of both metals inside the particle core. Batch experiments with a minimum nanocatalyst loading of 3 g/L showed complete dye degradation after 10 min of reaction time. The degradation efficiency was linearly dependent on the initial dye concentration, pH of the solution and total Fe-Ni catalyst concentration. The efficiency increased with increasing Fe-Ni concentration and decreasing pH of the solution, but decreased with an increase in the dye concentration. The degradation rate followed first order reaction kinetics with respect to the dye concentration. High performance liquid chromatography–mass spectrometry (HPLC–MS) analysis of the degradation products revealed that the degradation mechanism proceeds through a reductive cleavage of the azo linkage resulting in the formation of aniline and surface-adsorbed naphthol amine derivatives. The latter are subsequently hydroxylated through an oxidative process.
© 2007 Elsevier B.V. All rights reserved.

Keywords: Iron; Nickel; Nanoparticles; Azo dye; Degradation

1. Introduction

Contamination of aqueous streams due to dyes emanated by textile, leather and printing industries is a major environmental problem. Azo dyes, which contain one or more azo bonds (–N=N–), are a major class of synthetic, colored organic compounds. It is estimated that about half a million tonnes of azo dyes are manufactured each year all over the world and account for nearly 50% of all dyes produced [1]. The azo linkage is the most labile portion of an azo dye molecule and is responsible for its carcinogenicity and toxicity. Its degradation also leads to the formation of carcinogenic aromatic amines [2]. These properties are of concern to environmental and other regulatory authorities around the world.

Different physico-chemical and biological approaches are employed for the removal of azo dyes from aqueous solution. Amongst these, adsorption methods, biological degradation, coagulation processes, ozonation and hypochlorite treatment have been extensively exploited. However, these methods are costly, inefficient and result in the production of secondary waste products that need further disposal [3–5].

Advanced oxidation processes (AOPs) utilizing Fenton and photo-assisted Fenton reactions are widely utilized for azo dye degradation [6]. Their effectiveness results from the generation of highly reactive hydroxyl radicals (OH$^\bullet$) that decolorize both soluble and insoluble dyes. However, generation of large volumes of iron sludge is a major demerit of the process. Photocatalytic degradation using titanium dioxide is also a technically viable clean-up process for dyes [7–10] but problems like low quantum yields and requirement of UV light hinder its widespread acceptance as a practical remediation technology.

---

* Corresponding author. Fax: +91 20 25651542.
 *E-mail address:* paknikar@vsnl.com (K.M. Paknikar).

Reduction of dye-stuffs using zero-valent iron metal (Fe^0) has gained prominence due to its low-cost, easy availability, effectiveness and ability to completely degrade contaminants [11,12]. Zero-valent iron powder has been shown to decolorize the solution containing azo dyes and enhance its biodegradability [13–16]. Zhang et al. [16] have reported enhanced decolorization of Acid Orange 7 using the synergistic effect achieved by combining zero-valent iron powder with ultrasound radiation. Most studies to date on azo dye decolorization have emphasized commercial grade zero-valent iron. However, nano-scale iron exhibits enhanced dye degradation activity due to small particle size and large surface area [17]. The use of nano-iron has already shown tremendous potential for transformation of chlorinated benzenes and polychlorinated biphenyls [18]. Further, the incorporation of a second, catalytic metal like Pd, Zn, Ni or Pt leads to enhanced degradation rates as compared to nano-iron alone [19–22]. Although various combinations of iron-based bimetallic nanoparticles have been used for degradation of chlorinated organic compounds [23–25] and nitroaromatics [26], degradation of dye-stuffs using these bimetallic nanoparticles remains an unexplored area.

The present work highlights the degradation efficiency of Fe-Ni with respect to azo dyes, specifically Orange G, extensively used in textile, pulp and paper industries. The studies clearly show that Fe-Ni nanoparticles rapidly degrade the dye molecule, leading to the formation of aniline and a naphthol amine as secondary metabolites. A possible degradation mechanism is also suggested.

2. Experimental

2.1. Synthesis of Fe-Ni nanoparticles

Synthesis of the nano-scale Fe-Ni bimetallic particles was carried out by using sodium borohydride ($NaBH_4$) as the reductant, according to the following reaction [27]:

$$2Fe^{2+}(Ni^{2+}) + 2H_2O + BH_4^-$$
$$\rightarrow 2Fe(Ni) \downarrow + BO_2^- + 4H^+ + 2H_2 \uparrow \qquad (1)$$
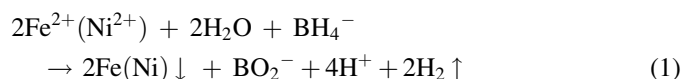
The nanoparticles were synthesized by the borohydride reduction of a 0.05 M aqueous mixture of $FeSO_4 \cdot 7H_2O$ (Loba Chemie, UK) and $NiCl_2 \cdot 6H_2O$ (Loba Chemie, UK). The solution of Fe^{2+} and Ni^{2+} species was stirred for 15 min without pH adjustment, followed by reduction using sodium borohydride (0.8 M) (Loba Chemie, UK) in 4-fold molar excess of the combined Fe^{2+} and Ni^{2+}. Nitrogen gas was circulated in the reaction vessel to prevent the accumulation of H_2 gas generated during the reduction process. An increase in the solution pH was observed when the borohydride was added in the solution and the final obtained value was ~10.0. During the reduction reaction, solution color was observed to change from brownish-green to black with dark colloidal particles. The solution was stirred for an additional 15 min and followed by vacuum filtration through 0.2 μm cellulose acetate filter paper. To get rid of the excess borohydride, the particles were washed with excess amount of deoxygenated water and rinsed with ethanol and acetone before being dried at 50 °C under vacuum overnight.

2.2. Characterization of nanoparticles

Brunnaer–Emmett–Teller (BET) surface area analysis of the synthesized nanoparticles was performed using nitrogen adsorption method with a surface analyzer model CHEM-BET-3000, Quantichrome Instruments, USA.

The morphology and size of the nanoparticles were estimated using a transmission electron microscope (TEM) (JEOL electron microscope Model 1200×) operated at an accelerating voltage of 120 kV. Samples were loaded on carbon-coated grids before being introduced into the vacuum chamber.

X-ray photoelectron spectroscopy (XPS) was carried out on a VG MicroTech ESCA 3000 instrument using Mg Kα radiation (photo energy 1253.6 eV) at pass energy of 50 eV and electron take off angle (angle between electron emission direction and surface plane) of 60°. The sample was placed in a container and was mounted on a sample probe taking care that the contact of air with sample was avoided. The sample was subjected to evacuation at 10^{-8} Torr during data collection. C 1s spectra have been used as a reference with binding energy value of 284.6 eV and the spectra of different samples were corrected for surface charging.

The total bulk iron and nickel concentration in the nanoparticles was determined using a flame atomic absorption spectrometer (AAnalyst 800, Perkin-Elmer, USA).

2.3. Batch degradation studies

Orange G (OG) was procured from Hi-Media Chemicals, UK and used without further purification. The structure of the azo dye is shown in Fig. 1. Dye stock solutions (350 mg/L) were prepared in deionized water and degradation experiments were performed in an open batch system at room temperature, 28 ± 2 °C. Dye solutions were stirred with an agitator to keep the nanoparticle powder suspended. Samples were withdrawn at fixed intervals for a few minutes and centrifuged for 5 min at 5000 rpm. The supernatant was pipetted out and the rate of
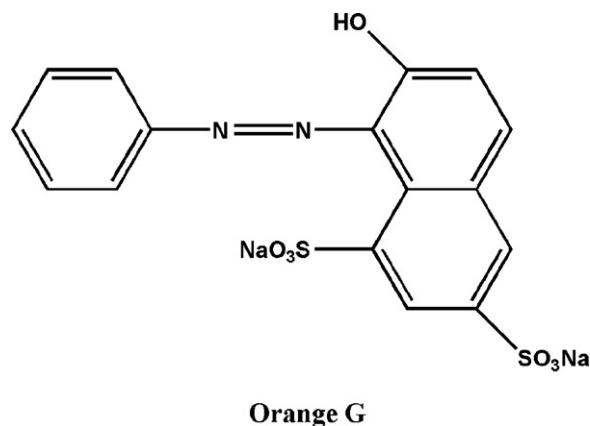

Orange G

Fig. 1. Chemical structure of Orange G.

degradation was monitored by measuring the absorbance of the solutions from 190 to 750 nm with a UV–vis spectrophotometer (ND1000, Nano Drop, UK).

2.4. Metabolite identification

The identification of degradation products in the solution was performed by high performance liquid chromatography–mass spectrometry (HPLC–MS) using a chromatographic system equipped with a UV detector set at 300 nm, and interfaced to a PE SCIEX model API3000 Triple Quadruple mass spectrometer equipped with a turbo ion spray interface. Samples were eluted at 1.5 mL/min through an Inertsil ODS 3 V column (5 μm, 150 mm × 4.6 mm) with the following gradient: from 0/100 (ammonium acetate 10 mM in acetonitrile/water) to 95/5 in 25 min, which was then maintained for 10 min. The interface conditions for the positive ion mode were as follows: nebulizer gas = 8 L/min, curtain gas = 12 L/min, needle voltage = 4500 V at 450 °C, orifice declustering potential = +10 V and focusing potential = 100 V. The flow from the HPLC-UV was split to allow 200 μL/min to enter the turbo ion spray interface.

3. Results and discussion

3.1. Nanoparticle characterization

The morphology and structure of the bimetallic nanoparticles is shown in the TEM images (Fig. 2). The nanoparticles are spherical in nature (size 20–40 nm) and connected in chains of beads. The formation of smaller sized particles is mainly due to the low molarity of Fe^{2+} and Ni^{2+} ions and a 4-fold excess molar excess of borohydride, which causes the rapid reduction rate of metal ions. Thus, more nuclei are generated and particle growth is controlled during the synthesis procedure. This produces Fe-Ni with low particle size and a BET surface area of 26 m^2/g.

XPS analysis of as-synthesized nanoparticles (Fig. 3) exhibited peaks at 712.0 and 725.1 eV, which are characteristic peaks for Fe^{2+} $2p_{3/2}$ and Fe^{2+} $2p_{1/2}$, respectively. A broader

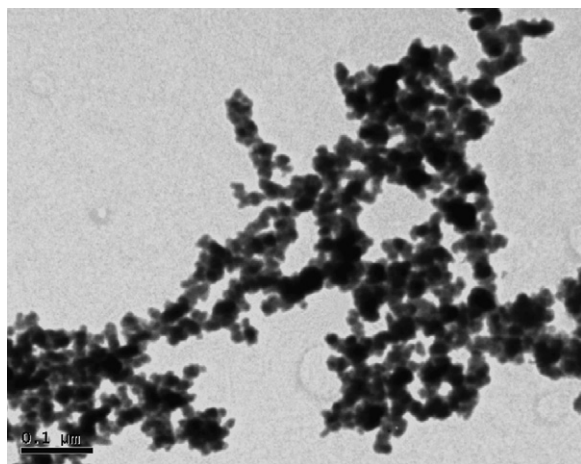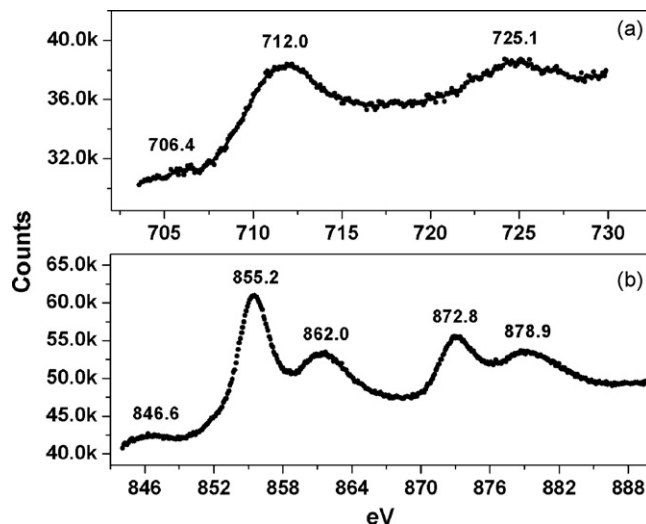Fig. 3. XPS analysis of as-synthesized Fe-Ni nanoparticles. (a) Fe 2p core level spectra and (b) Ni 2p core level spectra. The black dots correspond to the charge corrected raw data and the black solid line denotes the smoothened data.

peak was observed at 706.4 eV, which is associated with zero-valent iron (Fe^0 $2p_{3/2}$). Additionally, peaks were observed at 846.6, 855.2 and 872.8 eV, with two satellite peaks at 862.0 and 878.7 eV. The peak at 846.6 eV is the characteristic feature of Ni^0 whereas the peaks at 855.2 and 872.8 eV are binding energies of Ni^{2+} $2p_{3/2}$ and Ni^{2+} $2p_{1/2}$, respectively. The appearance of two strong satellite features, corresponding to Ni^{2+} $2p_{3/2}$ (862.0 eV) and Ni^{2+} $2p_{1/2}$ (878.7 eV) signals indicated the presence of electron correlation in the system.

The total bulk metal concentration, determined by AAS, was 26.3% (Fe) and 31.2% (Ni).

3.2. Azo dye degradation

The kinetics of Orange G degradation using Fe-Ni nanoparticles was studied using UV–vis spectroscopy. The decrease in the dye absorbance with time indicated Fe-Ni
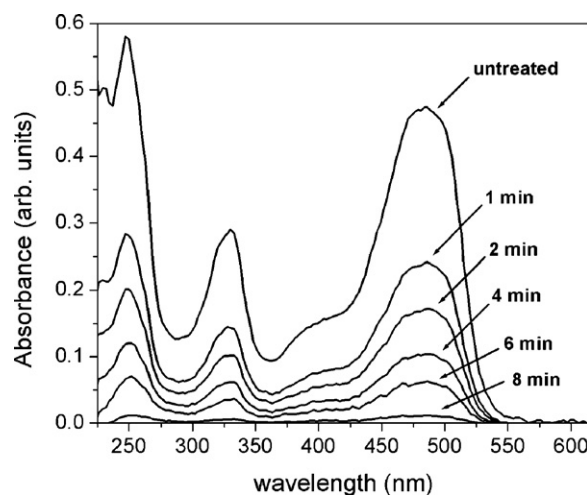
Fig. 2. TEM image of Fe-Ni bimetallic nanoparticles.

Fig. 4. Variation in optical absorption spectra of Orange G with reaction time using Fe-Ni nanoparticles. [Fe-Ni] = 3 g/L and [Dye] = 150 mg/L.
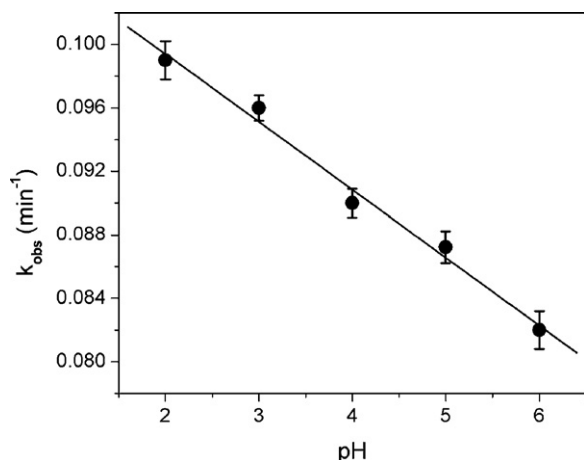
Fig. 5. Variation of degradation rate constant with pH. [Fe-Ni] = 3 g/L and [Dye] = 150 mg/L.

nanoparticles completely degraded Orange G in aqueous solution after 10 min (Fig. 4). The degradation of Orange G followed a first order kinetic model:

$$C = C_0 \exp(-k_{obs}t) \quad (2)$$

where C is the dye concentration at time t, C_0 is the initial dye concentration and k_{obs} is the first order rate constant. From the observed data, the calculated rate constant was 0.087 ± 0.02 min^{-1}.

3.3. Effect of pH on the degradation of Orange G

The pH of the aqueous solution is a complex parameter since it is related to the ionization state of the nanoparticle surface and that of the reactants and products such as acids and amines. Since the Fe-Ni nanoparticles are not active under alkaline conditions due to formation of a hydroxide layer on the particle surface, the effect of pH on dye degradation was evaluated in the 2–6 range. The kinetics of Orange G degradation at different pH values is depicted in Fig. 5. It can be seen that the degradation efficiency increased with decreasing pH, and a
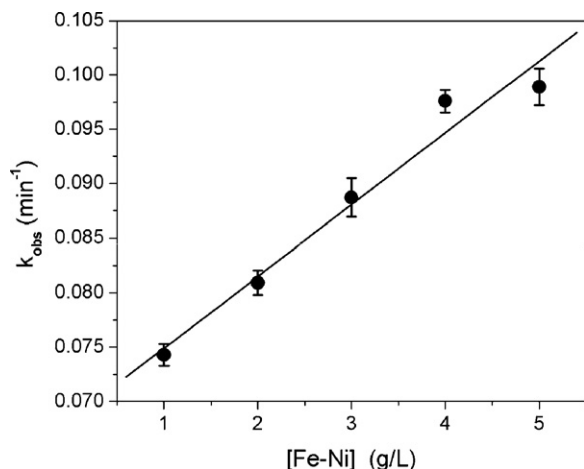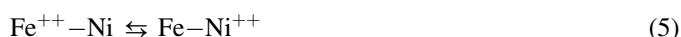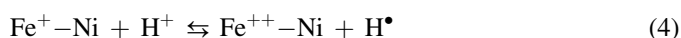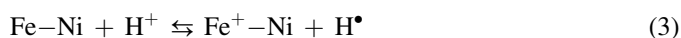

Fig. 6. Variation of degradation rate constant with Fe-Ni mass concentration. [Dye] = 150 mg/L.

maximum efficiency was observed at pH 2 ($\sim$99% efficiency in 3 min). Concomitantly, the rate constant decreased with an increase in the solution pH. The corrosion of iron in aqueous solution induces the formation of atomic hydrogen and subsequently molecular hydrogen at the Ni surface. This step is crucial for the reductive degradation of Orange G through its effective adsorption on the nanoparticle surface followed by hydride transfer from the nickel site. The formation and transfer of hydride on the nickel surface is effectively governed by the adsorption of hydrogen ions from water [28]. With decreasing pH, i.e., with increasing acidity, the increased H^+ concentration would result in an increase in nickel hydride formation, thereby increasing the degradation efficiency. Thus, the increase in the degradation efficiency of Fe-Ni nanoparticles at low pH can be explained on the basis of the following reactions occurring on the nanoparticle surface:

$$Fe-Ni + H^+ \leftrightarrows Fe^+-Ni + H^\bullet \quad (3)$$

$$Fe^+-Ni + H^+ \leftrightarrows Fe^{++}-Ni + H^\bullet \quad (4)$$

$$Fe^{++}-Ni \leftrightarrows Fe-Ni^{++} \quad (5)$$

$$H^\bullet + H^\bullet \leftrightarrows H_2 \quad (6)$$

$$2Fe-Ni + H_2 \leftrightarrows 2Fe-Ni-H \quad (7)$$

3.4. Effect of Fe-Ni concentration on the degradation of Orange G

Since the degradation of azo dye occurs at the Fe-Ni–H_2O interface, the surface area of the nanoparticles would certainly affect the degradation rate. An increase in the Fe-Ni nanoparticle concentration would simultaneously increase the number of active sites and the reactive surface area leading to enhanced dye degradation. Fig. 6 shows the change in degradation rate constant with increasing Fe-Ni concentration. Although the observed rate constant (k_{obs}) increases linearly with Fe-Ni concentration (Fig. 6), the relationship between k_{obs} and [Fe-Ni] is not first order. For instance, at a Fe-Ni concentration of 1 g/L, the k_{obs} value is 0.074 min^{-1}. A first order relationship would require that a 2-fold increase in Fe-Ni loading result in a 2-fold increase in the value of k_{obs}. However, a k_{obs} value of 0.081 min^{-1} is obtained at 2 g/L nanoparticle concentration. This non-linear relationship between reaction rate and catalyst loading has also been observed in granular iron systems for reductive degradation of polyhalogenated alkane reduction [29].

3.5. Effect of initial dye concentration on the degradation of Orange G

Five different concentrations of dye aqueous solutions (100, 150, 200, 250 and 300 mg/L) were employed at a fixed Fe-Ni concentration (3 g/L). Fig. 7 indicates that the degradation rate constant decreased with an increase in the initial dye concentration. The reduction of Orange G in Fe-Ni particulate system is a heterogeneous reaction, which involves adsorption
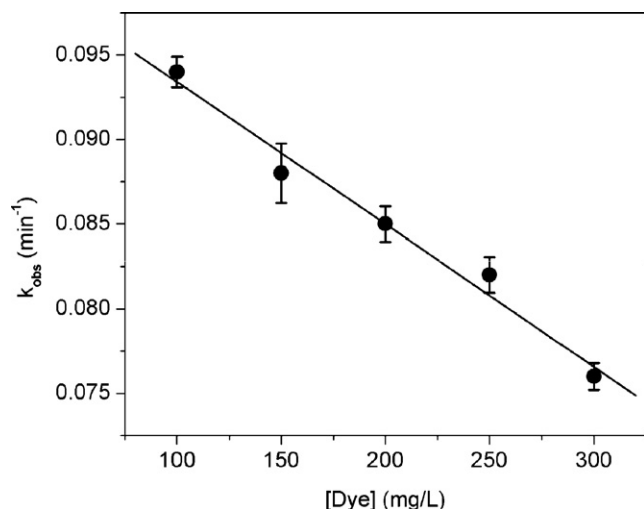
Fig. 7. Variation of degradation rate constant with initial dye concentration. [Fe-Ni] = 3 g/L.
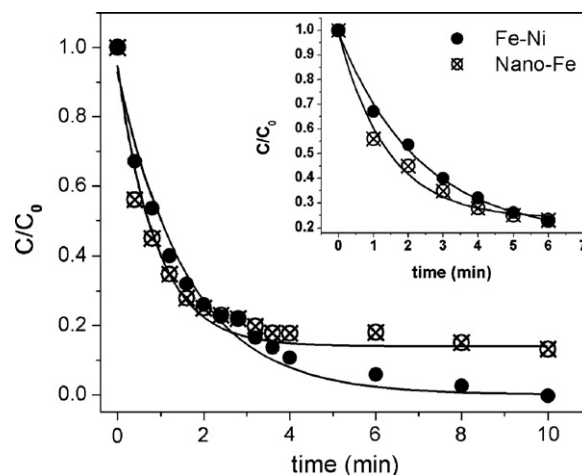

Fig. 8. Comparative kinetics of Orange G degradation using nano-Fe and Fe-Ni nanoparticles. [nano-Fe/Fe-Ni] = 3 g/L and [Dye] = 150 mg/L. Inset shows that nano-Fe degrades Orange G more rapidly at shorter reaction times.

of the dye on the nickel surface and the subsequent surface reaction. Since, the adsorption capacity of nickel is finite at a fixed concentration of Fe-Ni nanoparticles, increasing the bulk dye concentration would lead to competitive adsorption between the dye molecules. This, in turn, would decrease the number of dye molecules adsorbed and reduced on the nickel surface, leading to a decrease in the degradation efficiency (and the degradation rate constant).

3.6. Comparative degradation of Orange G using nano-Fe and bulk iron powder

Commercial iron powder (300 mesh, Merck Chemicals, UK) was pretreated with 6 M HCl for 10 min and washed with ultrapure water for 4 times to remove the residual HCl and Fe^{2+}. The degradation efficiency of bulk iron powder was only 31% after 10 min, and reached a saturated value of 40% after 30 min (data not shown).

The degradation efficiency of the Fe-Ni nanoparticles was also compared with iron nanoparticles (Fig. 8). Iron nanoparticles, having a BET surface area of 90 m^2/g, were prepared using the same synthetic procedure employed for bimetallic Fe-Ni nanoparticles. Although, iron nanoparticles showed enhanced degradation efficiencies at lower reaction times (inset of Fig. 8), the degradation efficiency of Fe-Ni nanoparticles is significant at higher reaction times. Moreover, iron nanoparticles did not achieve 100% degradation efficiency after 10 min, as compared to Fe-Ni nanoparticles. The lower catalytic efficiency of nano-Fe suggested that the presence of Ni plays a crucial role in the surface activity of Fe-Ni nanoparticles. Since the surface area of nano-Fe is almost 3 times more than that of Fe-Ni nanoparticles (90 and 26 m^2/g, respectively), dye degradation using iron nanoparticles proceeds rapidly as the reaction progresses. However, simultaneously, corrosion of the iron surface would lead to the formation of a surface-passivating iron oxide layer. Since the rate of corrosion is more rapid than the catalytic reduction process, the catalytic efficiency of nano-Fe decreases with

increasing reaction time (Fig. 8). This indicates that the surface passivation dominates the overall reduction process and hinders the hydride formation at the iron surface. On the other hand, the presence of Ni (which has lower hydrogen overpotential than Fe) in Fe-Ni bimetallic system not only accelerates hydrogen evolution, but also prevents the development of an oxide film by forming a Fe-Ni redox couple on the nanoparticle surface.

3.7. Efficiency of the recycled catalyst

In order to investigate the economy of the reductive degradation process, which is a measure of the number of times a catalyst can be reused without sacrificing its efficiency, the life span of Fe-Ni nanoparticles was tested. After the first degradation cycle, the treated solution was kept standing for a fixed time duration and then the supernatant was decanted. The nanoparticles were washed thoroughly with distilled water and reused for degradation of a fresh dye solution. All experiments were performed at fixed pH and dye concentration values. The results are presented in Table 1. It was found that the reactivity of the nanoparticles decreased as the time progressed. The activity of the nanocatalysts did not change significantly for 3 days. On the fifth day, it decreased by 12%, and on the tenth day, it decreased by 22%. However, the catalytic activity remained

Table 1
The life span of Fe-Ni bimetallic nanoparticles[a]

No.	k_{obs} (min^{-1})
(1)	0.087
(2)	0.085
(3)	0.077
(4)	0.065

(1) As-synthesized Fe-Ni nanoparticles; (2) Fe-Ni nanoparticles dipped in degraded dye solution for 3 days before use; (3) Fe-Ni nanoparticles dipped in degraded dye solution for 5 days before use; (4) Fe-Ni nanoparticles dipped in degraded dye solution for 10 days before use.

[a] All data are average values of three parallel determinations.

constant after 10 days, indicating that the Fe-Ni nanoparticles possess a considerably long reactive life span.

It is very well understood that iron corrosion in water is more rapid than in air, due to the presence of hydroxyl ions and dissolved oxygen, which can attack the bulk metal and form iron hydroxides and oxides on the surface. The hydroxides are easily leached out from the surface and this exposes the inner layer of core metal for further attacks, resulting in loss of the metallic iron and reduction in the catalytic efficiency.

Although, the presence of nickel prevents the formation of an iron oxide layer, the Fe-Ni electrochemical cell on the surface would be active for a certain period only, i.e., till nickel remains in the zero-valent state. Once all the nickel atoms are ionized, the iron corrosion process would dominate the reaction process and control the catalytic efficiency of the Fe-Ni system. Such a hypothesis is further corroborated by monitoring the changes in the surface characteristics of Fe-Ni nanoparticles by comparing the XPS spectra of as-synthesized and reused catalyst (Fig. 9).

The striking feature of the XPS spectrum of reused nanoparticles is the presence of peaks at 856.0 and 862.5 eV, characteristic of Ni $2p_{3/2}$ and Ni $2p_{1/2}$, respectively, and a small broad peak at 846.9 eV, due to surface migrated Ni^0 species. The appearance of two strong satellite features, corresponding to Ni $2p_{3/2}$ (862.2 eV) and Ni $2p_{1/2}$ (879.8 eV) signals indicated the presence of electron correlation in the system. In addition, the shifting of the Fe^0 peak on the lower energy side as compared to as-synthesized nanoparticles indicated the establishment of a Fe/Ni electrochemical cell on the surface of the nanoparticles. Formation of an electrochemical cell is triggered by the corrosion of iron in water and continuous exposure of the nanoparticles to water during the recycling experiments would lead to an oxide layer formation and affect the catalytic efficiency of Fe-Ni system. In other words, the catalytic performance would decrease after a certain water-exposure period, as observed in Table 1. However, these nanoparticles still show a much faster degradation profile, compared to commercially available iron powder (material of choice for field-level technology).
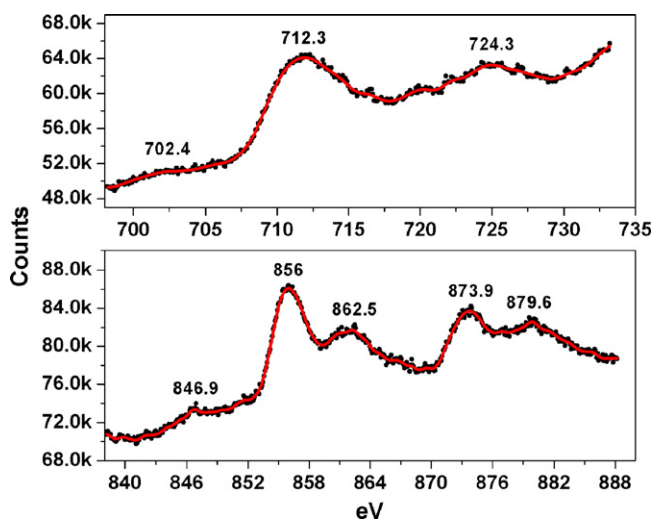
3.8. Degradation mechanism and identification of metabolites

In order to provide supportive evidences for the proposed degradation hypothesis, identification of degradation intermediates was carried out using separate HPLC–MS analysis of the treated dye solution and the products adsorbed on the nanoparticle surface. HPLC–MS analysis of the treated dye solution ([Dye] = 100 mg/L and [Fe-Ni] = 3 g/L) showed the complete absence of any degradation products. This preliminary evidence indicated that Fe-Ni nanoparticles completely mineralized the azo dye into CO_2. GC-TCD analysis of the reaction headspace, however, did not corroborate the presence of CO_2 as the major degradation product. In order to establish the exact mechanism of dye degradation, the concentration of dye solution was increased (correspondingly nanoparticle concentration was increased to maintain same dye:catalyst ratio) to obtain a strong signal in
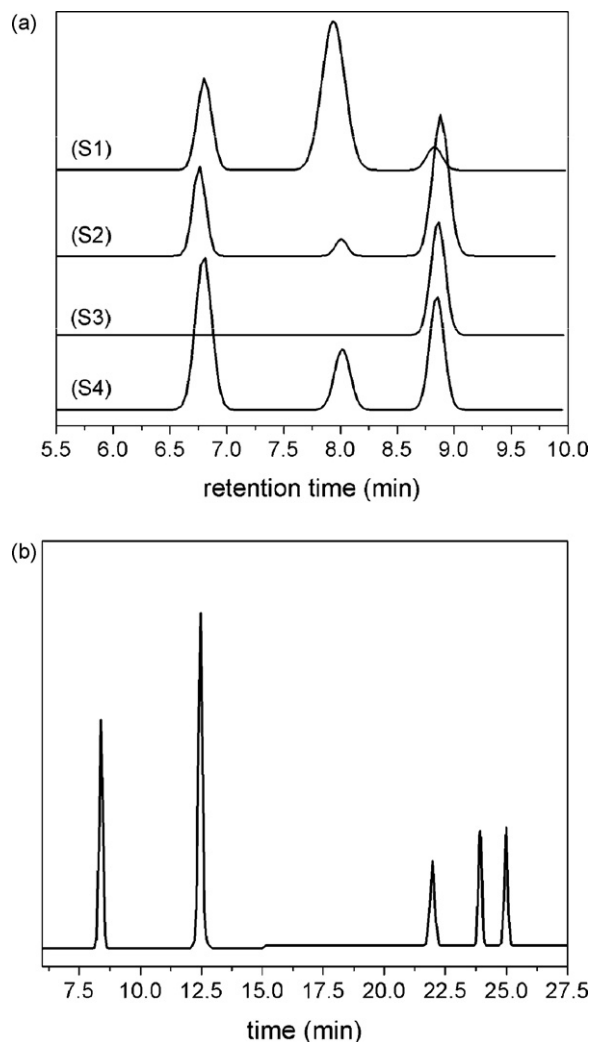

Fig. 10. (a) HPLC–MS analysis of Orange G degradation products. (S1) [Dye] = 5000 mg/L, [Fe-Ni] = 10 g/L; (S2) [Dye] = 5000 mg/L, [Fe-Ni] = 30 g/L; (S3) [Dye] = 5000 mg/L, [Fe-Ni] = 60 g/L; (S4) [Dye] = 10,000 mg/L, [Fe-Ni] = 60 g/L; (b) HPLC–MS analysis of Orange G degradation metabolites adsorbed on the surface of Fe-Ni nanoparticles.

Fig. 9. XPS analysis of used Fe-Ni nanoparticles exposed to air for 3 days.
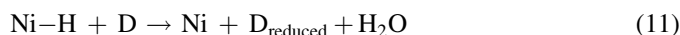
Table 2
Proposed chemical structures of Orange G degradation products identified by HPLC–MS

S. No.	Retention time (min)	Molecular weight	Proposed chemical structure
(S1)	6.79	409	$C_{16}H_{13}N_2O_7S_2$ (protonated dye)
	7.93	408	$C_{16}H_{12}N_2O_7S_2$ (residual dye)
	8.82	93	$C_6H_5NH_2$ (aniline)
(S2)	6.76	409	$C_{16}H_{13}N_2O_7S_2$ (protonated dye)
	8.03	408	$C_{16}H_{12}N_2O_7S_2$ (residual dye)
	8.88	93	$C_6H_5NH_2$ (aniline)
(S3)	8.86	93	$C_6H_5NH_2$ (aniline)
(S4)	6.81	409	$C_{16}H_{13}N_2O_7S_2$ (protonated dye)
	8.01	408	$C_{16}H_{12}N_2O_7S_2$ (residual dye)
	8.85	93	$C_6H_5NH_2$ (aniline)

the LC–MS scans. Accordingly, three samples were chosen: (S1) [Dye] = 5000 mg/L + [Fe-Ni] = 10 g/L; (S2) [Dye] = 5000 mg/L + [Fe-Ni] = 30 g/L; and (S3) [Dye] = 5000 mg/L + [Fe-Ni] = 60 g/L. Sampling for all LC–MS scans were performed under constant reaction volume and kinetics. The results of the LC–MS studies are shown in Fig. 10a and the proposed chemical structures of the degradation products are listed in Table 2.

HPLC–MS analysis of sample S1 showed the presence of two species: protonated dye and aniline along with the undegraded dye. However, increasing the amount of nanoparticles to 30 g/L (sample S2) and 60 g/L (sample S3) resulted in complete degradation of all parent and protonated dye molecules, leaving behind only aniline as the end product. The presence of protonated dye species as an intermediate product

was further confirmed by treating 10,000-mg/L dye solution with 60 g/L Fe-Ni nanoparticles (sample S4). The HPLC–MS results indicated that Orange G degradation using Fe-Ni nanoparticles generates aniline and a naphthol amine through reductive cleavage of the azo linkage. However, the naphthol amine could not be detected in aqueous supernatant (Fig. 10a). To identify whether it is adsorbed on the Fe-Ni nanoparticle surface, the treated dye solution was centrifuged and the supernatant was discarded. The nanoparticles were dried and surface adsorbed metabolites were extracted in acetonitrile. HPLC–MS analysis (Fig. 10b) of this extract exhibited the presence of the anticipated naphthol amine derivative as well as different hydroxylated species, which are summarized in Table 3.

The heterogeneous catalytic degradation of Orange G with Fe-Ni bimetallic nanoparticles proceeds *via* surface reactions involving both Fe and Ni active sites as given below:

$$Fe^0 \rightarrow Fe^{2+} + 2e^- \tag{8}$$

$$2H_2O + 2e^- \xrightarrow{Ni} 2H^* + 2OH^- \tag{9}$$

$$Ni + H^* \rightarrow Ni-H \tag{10}$$

$$Ni-H + D \rightarrow Ni + D_{reduced} + H_2O \tag{11}$$

In the above-described mechanism, iron corrodes galvanically, resulting in the formation of nickel hydride. The nickel hydride then reductively degrades the dye (D) by cleaving the azo linkage, whereby a hydride-free nickel surface is formed to adsorb newly generated H^* (atomic hydrogen).

Compared to nickel, iron corrodes rapidly and galvanically protects nickel in a bimetallic couple. Thus, metallic nickel can lose electrons to reduce the dye through a monometallic
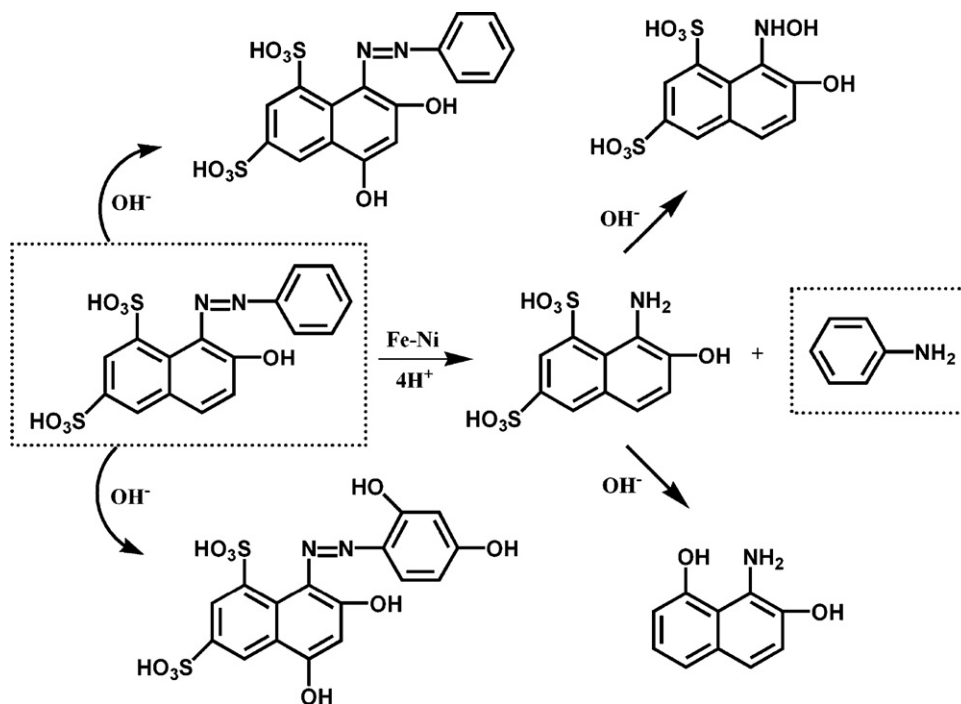

Fig. 11. Proposed mechanistic pathways of Orange G degradation. The products postulated are based on the analysis of the HPLC–MS data only. Dotted squares indicate products found in the supernatant only.

Table 3
Proposed chemical structures of Orange G degradation products adsorbed on the surface of Fe-Ni nanoparticles

Retention time (min)	Molecular weight	Proposed chemical structure
8.34	454	
12.39	316	
21.94	333	
23.9	174	
24.95	423	

mechanism (Eq. (12))

$$Ni^0 + D + H_2O \rightarrow Ni^{2+} + D_{reduced} + OH^- \qquad (12)$$

The nickel ion, thus formed, is reduced to metallic nickel by electron released by Fe/Fe^{2+} and Fe^{2+}/Fe^{3+} redox reactions. Thus, dye reduction at the nickel surface will continue as long as there exists an electronic bridge between the two metals. This alternate pathway for dye degradation is illustrated below:

$$Fe^0 \rightarrow Fe^{2+} + 2e^- \qquad (13)$$

$$Ni^{2+} + 2e^- \rightarrow Ni^0 \qquad (14)$$

Under such a condition, it is quite likely that the degradation mechanism for Orange G involves both oxidative and reductive pathways operating simultaneously in the presence of Fe-Ni

nanoparticles as catalyst. However, the initiation of the degradation process predominantly occurs *via* a reductive pathway and subsequently would lead to oxidative mechanism as the reaction progresses with time. Thus, the rate of iron corrosion would eventually trigger the second pathway once the reductive process is inhibited by the formation of oxide layer and cessation of hydride formation. The presence of Ni not only accelerates iron corrosion leading to increased hydrogen evolution but also prevents the formation of an oxide film thus blocking the reactive sites on the Fe surface. Such a feature has already been noted for Ni catalysts wherein the key step in hydrogenation of nitroamines [30] and carbon tetrachloride [31] is the generation of powerful reducing agent such as active hydrogen on the Ni surface.

The formation of hydroxylated products mainly arises from the attack of the hydroxyl ions (generated in Eqs. (9) and (12))

on the surface adsorbed species formed by the azo cleavage. Since, the products of reductive dye degradation (aniline and naphthol amine derivatives) cannot be further reduced, they can react with the hydroxyl ions present on the particle surface. But, only the surface adsorbed species would undergo hydroxylation as hydroxyl ions have a strong affinity to iron. Since, aniline was detected in the supernatant, formation of amino phenols on the particle surface was not possible, which was confirmed by their absence in the HPLC–MS analysis. On the other hand, the naphthol derivative and a fraction of the dye molecules remained adsorbed on the nanoparticle surface, making them vulnerable to hydroxylation.

On the basis of the HPLC–MS results, a plausible mechanism of degradation for Orange G is summarized in Fig. 11, which outlines two different pathways involving reductive cleavage of azo linkage and hydroxylation of naphthol amine species.

4. Conclusion

This study demonstrates the reductive degradation of an azo dye, Orange G, using Fe-Ni bimetallic nanoparticles in aqueous solution. The rapid degradation of the dye solution was monitored spectrophotometrically and was found to fit the first order kinetic model. Kinetics of dye degradation showed that the solution pH, Fe-Ni mass concentration and the initial dye concentration are the main factors that influence the degradation rates. With increasing acidity and nanoparticle concentration, the degradation rate increased linearly. HPLC–MS analysis of degradation metabolites revealed the reductive cleavage of the azo linkage to produce aniline and naphthol amine derivatives with the latter remaining adsorbed on the particle surface. The nano-scale particles also demonstrated an enhanced dye degradation rate compared to both commercial micro-scale Fe powder and iron nanoparticles. The latter was due to the presence of catalytic Ni, which improved the performance of the catalyst by producing more reducing species on the bimetallic surface. More importantly, these nanoparticles showed a significantly long life span with sustained reactivity, making them potential candidates for dye degradation technologies. However, the implications of this study with respect to treatment of real wastewaters from the dye industries are mixed: although the degradation of Orange G is very rapid, the resulting products are non-degradable, toxic aromatic amines (aniline and naphthol amines) that are of regulatory concern and require further treatment. To reach the dye wastewater emission standard, a combination of Fe-Ni nanoparticle-based treatment with other wastewater treatment technologies like advanced oxidation processes (AOPs) or bioremediation would be a viable option.

References

[1] J. Cao, L. Wei, Q. Huang, L. Wang, S. Han, Chemosphere 38 (1999) 565–571.
[2] K. Golka, S. Kopps, Z.W. Myslak, Toxicol. Lett. 151 (2004) 203–210.
[3] Z. Sun, Y. Chen, Q. Ke, Y. Yang, Y. Yuan, J. Photochem. Photobiol. A 149 (2002) 169–174.
[4] K. Tanaka, K. Padermpole, T. Hisanga, Water Res. 34 (2000) 327–333.
[5] S.H. Lin, F.C. Peng, Water Res. 30 (1996) 587–592.
[6] I.K. Konstantinou, T.A. Albanis, Appl. Catal. B 49 (2004) 1–14.
[7] M.R. Hoffmann, S.T. Martin, W. Choi, D.W. Bahnemann, Chem. Rev. 95 (1995) 69–96.
[8] M. Janus, A.W. Morawski, Appl. Catal. B 75 (2007) 118–123.
[9] B. Wawrzyniak, A.W. Morawski, Appl. Catal. B 62 (2006) 150–158.
[10] R. Comparelli, E. Fanizza, M.L. Curri, P.D. Cozzoli, G. Mascolo, R. Passino, A. Agostiano, Appl. Catal. B 55 (2005) 81–91.
[11] S. Nam, P.G. Tratnyek, Water Res. 34 (2000) 1837–1845.
[12] T.L. Johnson, M.M. Scherer, P.G. Tratnyek, Environ. Sci. Technol. 30 (1996) 2634–2640.
[13] J. Cao, L. Wei, Q. Huang, L. Wang, S. Han, Chemosphere 36 (1999) 565–571.
[14] J.R. Perey, P.C. Chiu, C.-P. Huang, D.K. Cha, Water Environ. Res. 74 (2002) 221–225.
[15] J.A. Mielczarski, G.M. Atenas, E. Mielczarski, Appl. Catal. B 56 (2005) 289–303.
[16] H. Zhang, L. Duan, Y. Zhang, F. Wu, Dyes Pigm. 65 (2005) 39–43.
[17] B.H. Moon, Y.B. Park, S.S. Kim, G.T. Seo, T.S. Lee, T.S. Kim, Mater. Sci. Forum 544–545 (2007) 705–708.
[18] Y. Xu, W. Zhang, Ind. Eng. Chem. Res. 39 (2000) 2238–2244.
[19] S.F. Cheng, S.C. Wu, Chemosphere 41 (2000) 1263–1270.
[20] J. Wang, P. Blowers, J. Farell, Environ. Sci. Technol. 38 (2004) 1576–1581.
[21] H.L. Lien, W.X. Zhang, Chemosphere 49 (2002) 371–378.
[22] B. Schrick, J.L. Blough, A.D. Jones, T.E. Mallouk, Chem. Mater. 14 (2002) 5140–5147.
[23] J.T. Nurmi, P.G. Tratnyek, V. Sarathy, D.R. Baer, J.E. Amonette, K. Pecher, C. Wang, J.C. Linehan, D.W. Matson, R.L. Penn, M.D. Driessen, Environ. Sci. Technol. 39 (2005) 1221–1230.
[24] Y. Liu, S.A. Majetich, R.D. Tilton, D.S. Sholl, G.V. Lowry, Environ. Sci. Technol. 39 (2005) 1338–1345.
[25] J. Quinn, C. Geiger, C. Clausen, K. Brooks, C. Coon, S. O'Hara, T. Krug, D. Major, W.-S. Yoon, A. Gavaskar, T. Holdsworth, Environ. Sci. Technol. 39 (2005) 1309–1318.
[26] S.H. Joo, A.J. Feitz, D.L. Sedlak, T.D. Waite, Environ. Sci. Technol. 39 (2005) 1263–1268.
[27] Y.-H. Tee, E. Grulke, D. Bhattacharyya, Ind. Eng. Chem. Res. 44 (2005) 7062–7072.
[28] F. Herrera, A. Lopez, G. Mascolo, P. Albers, J. Kiwi, Appl. Catal. B 29 (2001) 147–162.
[29] D.M. Cwiertny, A.L. Roberts, Environ. Sci. Technol. 39 (2005) 8948–8957.
[30] L. Gui, R.W. Gillham, M.S. Odziemkowski, Environ. Sci. Technol. 34 (2000) 3489–3494.
[31] J. Wang, J. Farell, Environ. Sci. Technol. 37 (2003) 3891–3896.